Three-dimensional time-dependent Hartree-Fock approach for arbitrarily oriented molecular hydrogen in strong electromagnetic fields

L. A. A. Nikolopoulos,* T. K. Kjeldsen, and L. B. Madsen
Lundbeck Foundation Theoretical Center for Quantum System Research, Department of Physics and Astronomy, University of Aarhus, 8000 Aarhus C, Denmark
(Received 17 April 2007; published 4 September 2007)

We present a theoretical framework for the electronic dynamics of arbitrarily oriented molecular hydrogen in strong and short electromagnetic fields. The ground state of H_2 is obtained by propagating the time-dependent Schrödinger equation in imaginary time by assuming the Hartree-Fock ansatz for the interaction between the electrons. The interaction of H_2 with the radiation field is considered in the single-active-electron approximation, with the continuum electron subject to Hartree-Fock radial potentials. We propagate the wave function by a split-operator scheme projected on a spherical harmonics basis. Alignment-dependent yields and angular distributions for one- and two-photon ionization induced by an external femtosecond light source are presented and compared with available theoretical results.

DOI: 10.1103/PhysRevA.76.033402 PACS number(s): 33.80.Rv, 42.50.Hz

I. INTRODUCTION

Understanding the fundamental processes that occur when atoms and molecules are subject to extreme conditions is currently a major research area. Experimentally, such processes are usually initiated by short intense laser pulses radiating at infrared wavelengths [1] or in the near future by the free electron laser which will provide intense ultraviolet light sources [2,3]. In addition to the fundamental interest in the interaction of molecules with intense and/or ultrashort electromagnetic fields [1,4], such processes have recently been utilized at a more practical level for reconstruction of nuclear probability distributions, visualization of molecular orbitals, alignment of molecules as well as production of high-order harmonics which in turn are used for the generation of ultra short fields at the subfemtosecond scale [4–10].

Undoubtedly, molecules due to their multicenter nature are more complex systems than atoms, thus making a theoretical description of the molecular energy-level structure a highly demanding task and, accordingly, in most cases a number of approximations are employed. In addition, there are processes that may occur during the interaction of molecules with electromagnetic (EM) fields with no counterpart in atomic systems. For instance, alignment and orientation of the molecule with respect to the external field affect the ionization and harmonic yield. Also the electronic wave function depends on the internuclear distance R and this may lead to enhanced ionization at particular values of R.

From a theoretical point of view, it is a tremendous task to treat the exact time-dependent response of a multielectron system subject to a strong oscillating field by *ab initio* methods. Considering the interaction with the EM field, most theoretical studies make use of the strong-field approximation (SFA) where the influence of the Coulomb potential on the ejected electron wave function is neglected in favor of the external field. With less severe approximations, an approach that adopts the single-active-electron (SAE) approximation was applied to the atomic case some time ago [11]. In the SAE approximation, the time-dependent Schrödinger equation (TDSE) for a single electron moving in the effective field generated by the nuclei and all the other electrons is solved numerically. SAE models where one reduces the dimensionality of the multielectron problem by freezing the most tightly bound electrons have proven to be very useful in cases where multiple electronic excitations are insignificant, and the SAE approximation is probably the most widely used approach when studying phenomena such as single ionization, above-threshold ionization (ATI) and high-harmonic generation (HHG).

Ab initio approaches of one-photon single- and double-ionization of H_2^+ have been developed [12–19]. In the multiphoton case the nonperturbative driving by the external field has impedeed fast progress. Lately, however, nonperturbative *ab initio* methods to solve the TDSE by a number of different techniques have been developed [20–24]. In most cases these approaches were developed, and applied first, to the case of the molecular hydrogen ion (H_2^+), being the simplest molecular system but also due to its fundamental importance [21,25–31]. Studies of multiphoton ionization of H_2 by solving the TDSE either by assuming the fixed nuclei approximation [23,32,33] or even including the electronic and vibrational degrees of freedom [34] have appeared in the literature only very recently. The solution of the TDSE for systems with more than two electrons and/or including nuclear degrees of freedom is computationally involved and necessitating thus the use of high-power computer resources [35]. Moreover in most cases, an important degree of freedom, namely the orientation of the molecular axis with respect to the field polarization has not been considered. The development of the alignment techniques have opened up yet another area of theoretical research. Experimentally, significant orientation dependence of the ionization and the harmonic yield production was observed [36,37]. Thus a number of important issues needs to be investigated and answered, namely the degree of influence of the molecular axis orientation to

*Present address: Department of Applied Mathematics and Theoretical Physics, The Queen's University of Belfast, BT7 1NN Belfast, UK.

certain quantities such as ionization, dissociation and harmonic yield, photoelectron energy spectra, etc.

Given our intention to study multielectron molecular systems under arbitrarily oriented intense EM ultrashort fields we are looking for methods that can treat multielectron molecules with the least approximations possible but at the same time are computationally tractable. Such approaches have been developed in atomic and molecular physics studies, and include time-dependent Hartree-Fock (TDHF) [11], time-dependent density functional theory (TDDFT) [38] to refer to the most representative ones.

Though in atomic and molecular systems there is a vast number of theoretical efforts in the spirit of TDHF [39–45], even some extensions to include correlation between the electrons, the question of how much and under what conditions correlation beyond the Hartree-Fock model is important still remains unanswered. The underlying reason is the difficulties introduced by the nonlinear nature of the TDHF equations in combination with the fact that the single-configuration ansatz and the excitation process induced by the EM field are inconsistent. Improvements of the restricted Hartree-Fock (RHF) ansatz such as the unrestricted HF (UHF) approach and inclusion of exchange effects appear to be possible solutions to overcome such problems, although the applications so far are only in one-dimensional (1D) models [46–49]. Recently a systematic approach, multiconfiguration TDHF, capable of treating multielectron excitations and to include correlations between the electrons (beyond HF) was developed [50] and applied to 1D system. Interestingly enough, when the same method was applied to the corresponding 3D system contradictions with the 1D results were found, a sign that conclusions based on 1D model systems should not be taken into account firmly [51].

In the present work, we undertake an investigation of a compromising problem. Confident by having applied the present split-operator technique to the ionization of the molecular hydrogen ion [31,52] we extend the method by treating the arbitrarily oriented H_2 in all its full dimensionality (3D for each electron) at the cost of describing the ionization process in the SAE approximation. We choose the H_2 molecule as a generic system of diatomic molecules with two electrons outside a closed shell. We are motivated by fundamental interest in dynamics of H_2 when exposed to an intense laser field but also this system offers a test bend for extending naturally our split-operator technique to other diatomic molecules, e.g., O_2 and N_2. The adoption of the SAE allows us to overcome two problems inherent in the TDHF approaches, namely (a) the nonlinearity of the time-dependent equations and (b) the inconsistency of a single-determinant expansion of the time-dependent wave function with the concept of the ionization process. As a result of the above we restrict our study to cases where no multiple excitations and/or double ionization play a crucial role in the dynamics of the ionization, a fact that depends on the system under consideration as well as the intensity, wavelength and pulse duration of the radiation field. In H_2 a TDHF 3D finite element (FE) calculation at 532 nm showed that the FE and the frozen core ionization rates differ by only 10% [44]. The TDHF approach that treat both electrons exact, within one dimension [48], show that one orbital ("the inner") stays localized and that there is negligible core excitation at equilibrium. Furthermore, the double ionization yield is proportional to the single ionization yield for intensities up to 10^{15} W/cm^2, but of much less magnitude [53]. In addition, the SAE can be systematically improved by considering a "frozen core" screened potential that takes into account the relaxation of the H_2^+ into its equilibrium position during ionization [33,54]. Hence, theoretically, a description in terms of a SAE model is expected to be fairly accurate and definitely to grasp the physics qualitatively. This way, we try to be as close as possible to the criteria that justify the SAE approximation, by choosing carefully the pulse characteristics.

For all the above reasons we believe that the present study, as a first attempt to treat an arbitrarily oriented molecular hydrogen in a strong ultrashort EM field as realistic as possible (also presenting in detail the technique) can provide, within its limits posed by the approximations discussed, a quantitative picture of the 3D ionization dynamics.

The paper is organized as follows. In Sec. II, we present the basic theoretical framework for the calculation of the ground state of H_2, the construction of the effective HF potential and the split-operator propagation technique of the time-dependent wave function. In Sec. III, we give the formulation related with the propagation of the active-electron wave function in the presence of an EM field with the polarization axis arbitrarily oriented with respect to the molecular axis. In Sec. IV, we present the method used to calculate ionization yield, energy and angular distribution of the photoelectron. In Sec. V, we apply the method to one- and two-photon ionization of molecular hydrogen exposed in a strong UV few femtoseconds EM field. Finally, in the Appendix, we have relegated much of the technical details.

In the presentation of the formulas, atomic units are used ($m=\hbar=|e|=a_0=1$) throughout.

II. FORMULATION

We consider a two-electron diatomic molecule with nuclear charges Z_A and Z_B and with the nuclei fixed at positions $\mathbf{R}_A$ and $\mathbf{R}_B$. By defining $r_{12}=|\mathbf{r}_1-\mathbf{r}_2|$ and $r_{iA}=|\mathbf{r}_i-\mathbf{R}_A|$, $r_{iB}=|\mathbf{r}_i-\mathbf{R}_B|$, we write the Hamiltonian governing the electronic dynamics as

$$H_e(\mathbf{r}_1,\mathbf{r}_2)=\sum_{i=1,2}\left[-\frac{1}{2}\nabla_i^2-\frac{Z_A}{r_{iA}}-\frac{Z_B}{r_{iB}}\right]+\frac{1}{r_{12}}. \tag{1}$$

The TDSE reads $[i(\partial/\partial t)-H_e-V_F]\Psi(\mathbf{r}_1,\mathbf{r}_2,t)=0$, with the field-molecule interaction in the dipole approximation given by

$$V_F(\mathbf{r}_1,\mathbf{r}_2,t)=\sum_{i=1,2}V_I(\mathbf{r}_i,t)=\sum_{i=1,2}\mathbf{E}(t)\cdot\mathbf{r}_i, \tag{2}$$

with $V_I(\mathbf{r}_i,t)=\mathbf{E}(t)\cdot\mathbf{r}_i$ and $\mathbf{E}(t)$ the electric field.

For the two-electron wave function of, e.g., H_2, we make the Hartree-Fock ansatz, and express the two-electron wave function as a product of single-electron orbitals, namely,

$$\Psi(\mathbf{r}_1,\mathbf{r}_2,t)=\psi_1(\mathbf{r}_1,t)\psi_2(\mathbf{r}_2,t), \tag{3}$$

with ψ_1 and ψ_2 each normalized to unity.

By inserting Eq. (3) in the TDSE, projecting over $\psi_i(\mathbf{r}_i,t)$ for $i=1,2$ and making the following transformation $\psi_i \rightarrow \psi_i \exp(i\int^t dt' \langle \psi_i | \partial\psi_i/\partial t' \rangle)$ we obtain a set of coupled equations for the time evolution of the single-electron orbitals

$$i\frac{\partial}{\partial t}\psi_i(\mathbf{r}_i,t) = [h_i + V_D^{(j)}(\mathbf{r}_i,t) + V_I(\mathbf{r}_i,t)]\psi_i(\mathbf{r}_i,t), \tag{4}$$

for $i,j=1,2$ and $i \neq j$. The single-electron Hamiltonian h_i for the ith electron reads

$$h_i = -\frac{1}{2}\nabla_i^2 + V_M(\mathbf{r}_i), \tag{5}$$

with the molecular potential $V_M(\mathbf{r}_i) = -Z_A/r_{iA} - Z_B/r_{iB}$. The Coulombic interaction between the two-electrons is reduced to a time-dependent mean-field potential felt by each of the electrons (averaged over the spatial variables of the other electron),

$$V_D^{(j)}(\mathbf{r}_i,t) = \int d^3\mathbf{r}_j \frac{|\psi_j(\mathbf{r}_j,t)|^2}{|\mathbf{r}_i - \mathbf{r}_j|}, \tag{6}$$

with $i,j=1,2$ and $i \neq j$.

A. Determination of the H_2 ground state orbitals

The Hartree ansatz for the ground state of H_2 ($Z_A=Z_B=1$) is to assume the field-free two-electron wave function be a product of two identical single-electron orbitals

$$\Psi_0(\mathbf{r}_1,\mathbf{r}_2,t) = \psi_0(\mathbf{r}_1,t)\psi_0(\mathbf{r}_2,t). \tag{7}$$

In this case $\psi_0=\psi_1=\psi_2$ and $V_I=0$ making the set of the coupled equations in Eq. (4) identical. Accordingly we are left with a single time-dependent equation

$$i\frac{\partial}{\partial t}\psi_0(\mathbf{r}_i,t) = \left(h_i + \int d^3\mathbf{r}\frac{|\psi_0(\mathbf{r},t)|^2}{|\mathbf{r}_i - \mathbf{r}|}\right)\psi_0(\mathbf{r}_i,t), \tag{8}$$

with $i=1,2$. In comparison with the TDSE for a single-electron system, we note the presence of an effective time-dependent inter-electronic potential given by Eq. (6) with $\psi_j=\psi_0$, which turns the TDSE into a non-linear differential equation. It is worth noting that the Hartree-Fock and the Hartree time-dependent equations give the same equations for the ground state. This follows since the exchange part of the Coulombic electron-electron interaction is simply half of the direct part of the inter-electronic potential.

The propagation procedure for the calculation of the ground state orbital of Eq. (8) is identical to the procedure used when the wave function is subject to an EM field (described in the next subsection) with the exception of two points: (i) The external EM field is set to zero, thus the wave functions are propagated under the molecular potential only. (ii) The real time step $\tau = t_{i+1} - t_i > 0$ is replaced by an imaginary step by making the substitution $\tau \rightarrow -i\tau$. Assuming that we start out from an arbitrary initial state it is well-known that propagation in imaginary time leads to the lowest energy eigenstate of the Hamiltonian. Propagation in imaginary time does not preserve the norm of the wave function, contrary to the norm changes with a rate which converges to the ground state eigenenergy as

$$E_g = \lim_{t\rightarrow\infty}\lim_{\tau\rightarrow 0} -\frac{1}{\tau}\ln\frac{\langle\psi(t+\tau)|\psi(t+\tau)\rangle}{\langle\psi(t)|\psi(t)\rangle}. \tag{9}$$

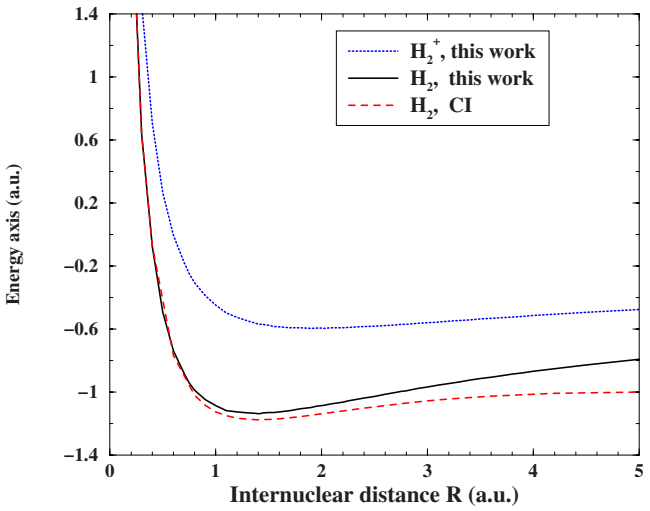

FIG. 1. (Color online) Potential curves for the H_2 and H_2^+. The full and the dashed line represent the H_2 ground state potential curve calculated within the present method and with a full configuration interaction (CI) method, respectively. The curve for the CI method has been taken from [12]. The dotted line is the exact potential curve for the H_2^+, calculated with the present approach.

In order to test the accuracy of our method we present in Fig. 1 the potential curves for H_2 and H_2^+ obtained by the present approach. The potential curve is defined as the electronic ground state energy plus the static nuclear repulsion energy for each fixed value of the internuclear distance. In the figure we also show the potential curve for H_2 obtained by a configuration-interaction method [12]. The agreement between the two curves is good at small internuclear distances and reasonable around the equilibrium position ($\sim$1.4 a.u.). The discrepancy becomes appreciable in the dissociation limit $R \rightarrow \infty$. This latter behavior is easy to understand: By using the wave function ansatz of Eq. (7), we restrict the two electrons to have the same functional dependence and explicitly neglect the ionic bonding part of the total wave function. The latter corresponds to an unequal sharing of the electronic charge, which in the dissociation limit leads to H^- and a proton. The ground state ansatz (covalent bonding part), which associates one electron with each nucleus, is expected to become more accurate at smaller internuclear distances. This is indeed the situation that is reflected by the behavior of the potential curve of H_2 obtained by the present method. As an additional test of the potential curve (of H_2), obtained with the present method, we have performed a restricted HF calculation [55] and found excellent agreement.

B. Propagation of H_2 in the SAE approximation

Let us now consider the TDSE of H_2 in an external radiation field. In the single-active electron approximation, one of

the electrons remains strongly bound, in fact untouched by the radiation field, while the other interacts with the field in the presence of a screened field due to the nuclei and the "frozen" electron. Thus if the energy of the initial ground-state orbitals ψ_0 is ε_0 the time evolution of the "frozen" orbital (let us assume the inactive electron to be represented by the orbital wave function ψ_1), is written as

$$\psi_1(\mathbf{r}_1,t) = \phi_0(\mathbf{r}_1)e^{-i\varepsilon_0 t}. \tag{10}$$

Inserting this expression into the set of the coupled TDSEs (4) results in an equation for the second orbital ($i=2$), with the direct time-*independent* (static) potential.

$$V_D^{(1)}(\mathbf{r}_2) = \int d^3\mathbf{r}_1 \frac{|\phi_0(\mathbf{r}_1)|^2}{|\mathbf{r}_2 - \mathbf{r}_1|}. \tag{11}$$

Let us, for notational convenience, drop the subscript from all dynamical observables that determine the evolution of the active electron and relabel $\mathbf{r}_2 \to \mathbf{r}$, $\psi_2(\mathbf{r}_2,t) \to \psi(\mathbf{r},t)$, $h_2 \to h$, $V_I(\mathbf{r}_2,t) \to V_I(\mathbf{r},t)$ and $V_D^{(1)}(\mathbf{r}_2) \to V_D(\mathbf{r})$, given that the Hamiltonian corresponds to a single-electron diatomic molecular system. In this case, the TDSE to be solved for the active electron is written as

$$i\frac{\partial}{\partial t}\psi(\mathbf{r},t) = [h + V_D(\mathbf{r}) + V_I(\mathbf{r},t)]\psi(\mathbf{r},t). \tag{12}$$

Compared with the single-electron molecular system (i.e., H_2^+), within the present SAE approximation, the presence of the extra electron, modifies the motion of the active electron by the addition of a static potential V_D in the ionic molecular Hamiltonian. Note that, within the SAE approximation the non-linearity of the TDHF equations is removed and the whole time-dependence of the potentials is due to the external EM field.

In our present numerical implementation, we choose a spherical coordinate system for the active electron [24,30,31]. We represent the angular variables in a basis of spherical harmonics and write the wave function as

$$\psi(\mathbf{r},t) = \sum_{l=0}^{\infty}\sum_{m=-l}^{l}\frac{f_{lm}(r,t)}{r}Y_{lm}(\theta,\phi). \tag{13}$$

In an actual calculation, we must truncate the spherical harmonics expansion at some maximum $l=l_{\max}$. In the remaining formulas we abbreviate the truncated double summation by Σ_{lm}. The radial functions f_{lm} which contain the time dependence are discretized on an equidistant radial grid.

The propagation of the wave function proceeds by using a split-operator spectral method in spherical coordinates (see Appendix A). If we assume the Hamiltonian $H(t)=h+V_D(\mathbf{r})+V_I(\mathbf{r},t)$, the formal evolution of the wave function from a time t_i by a time step τ, is given as $\psi(\mathbf{r},t_{i+1}) \approx \exp[-iH(\bar{t})\tau]\psi(\mathbf{r},t_i)$, where $\tau=t_{i+1}-t_i$ and $\bar{t}=(t_i+t_{i+1})/2$. In the present case, we separate the Hamiltonian into three terms, namely the radial kinetic ($T_r=-(1/2)\partial^2/\partial r^2$), centrifugal ($T_l=L^2/2r^2$) and the potential $[V(\mathbf{r},t)=V_M(\mathbf{r})+V_D(\mathbf{r})+V_I(\mathbf{r},t)]$ terms. Then, within the split-operator technique the wave function propagates as

$$r\psi(\mathbf{r},t+\tau) = e^{-iT_r(\tau/2)}e^{-iT_l(\tau/2)}e^{-iV(\bar{t})\tau}e^{-iT_l(\tau/2)}e^{-iT_r(\tau/2)}r\psi(\mathbf{r},t).$$

The error in the propagation scheme above is approximately cubic in τ and occurs mainly due to the splitting of noncommuting operators.

By projecting Eq. (13) on the spherical harmonic basis $Y_{lm}(\theta,\phi)$ we obtain a propagation scheme for each element of the radial functions $f_{lm}(r)=r\langle lm|\psi\rangle$ as

$$f_{lm}(r,t_{i+1}) = U_r U_l \sum_{l'm'} U_{lm;l'm'} U_{l'} U_r f_{l'm'}(r,t_i). \tag{14}$$

The above propagation scheme represents the central evolution formula of the present split-operator scheme applied in a spherical harmonic basis. In Eq. (14), the radial time-evolution operators are

$$U_r = e^{-i[-(1/2)(\partial^2/\partial r^2)](\tau/2)}\delta_{ll'}\delta_{mm'}, \tag{15}$$

$$U_l = e^{-i[l(l+1)/2r^2](\tau/2)}\delta_{ll'}\delta_{mm'}, \tag{16}$$

$$U_{lm;l'm'} = \langle lm|e^{-iV(\mathbf{r},\bar{t})\tau}|l'm'\rangle. \tag{17}$$

The quantity $U_{lm;l'm'}$ describes the evolution of the wave function due to the potential and the external field. As it is obvious from the above split-operator scheme this operator describes the mixing between the different partial waves in the expansion of the wave function. The technical details of the treatment of the operators Eqs. (15)–(17) are discussed in the Appendix A, (see also Ref. [31]).

III. PROPAGATION WITH EM FIELD OF ARBITRARY ORIENTED POLARIZATION AXIS

For arbitrary orientation of the linear field polarization vector with respect to the molecular axis, defined by the Euler angles (α,β,γ), the wave function in the two different frames is related through a rotation as $\psi^L(\mathbf{r}',t) = D(\omega)\psi^M(\mathbf{r},t)$, where $\omega=(\alpha,\beta,\gamma)$, $D(\omega)$ the Wigner rotation operator and $\mathbf{r}'=(r',\theta',\phi')$ the position vector expressed in the laboratory frame. Note that for rotation operations, $r'=r$. The Euler angle α corresponds to rotation around the polarization vector, β is the angle between the polarization and molecular axes, while γ is a rotation around the molecular axis.

Given that the diatomic molecule is rotationally symmetric around its own axis, the results are independent on the angle γ, thus we can set it to zero. However the dependence of the results on the angle α is less obvious since we have chosen to express our wave function in the molecular frame. For the same value of β we can have different orientations corresponding to different values of α. Such geometries will lead to different results, e.g., for, angular distributions of photoelectrons observed in the laboratory fixed frame. The linearly polarized field is, however, cylindrically symmetric around the z^L axis, and therefore the two different angular distributions will only differ by a trivial rotation around the z^L axis. To see this let us write the wave function in the laboratory frame by employing an arbitrary Wigner rotation

by an angle ω which is known to transform the spherical harmonic functions as [56]

$$Y_{lm}(\theta,\phi)=\sum_{m'} D^{(l)}_{mm'}(\omega)Y_{lm'}(\theta',\phi'). \tag{18}$$

By using the above formula and noting that $D^{(l)}_{m'm}(\omega)=\exp(-i\alpha m')d^{(l)}_{m'm}(\beta)\exp(-i\gamma m)$, we obtain

$$\psi^{(L)}(\mathbf{r}')=\sum_{lm'}\frac{1}{r'}f_{lm'}(r')e^{-i\alpha m'}Y_{lm'}(\theta',\phi'), \tag{19}$$

with $f_{lm'}(r')=\Sigma_m f_{lm}(r)\exp(-i\gamma m)d^{(l)}_{m'm}(\beta)$. From the above expression it easy to see the trivial phase dependence of the laboratory-expressed wave function on the angles α and γ due to axial symmetry along the polarization and the molecular axis, respectively. Thus, we conclude that the only nontrivial geometric dependence will be upon the angle β which defines the angle between the molecular and the laboratory axis. Therefore, we choose $\omega=(0,\beta,0)$ and make (a) a rotation by the angle β of the wave function into its laboratory frame, then (b) we propagate the wave function into the laboratory frame, and finally (iii) make a backward transformation into the molecular frame. The above propagation procedure for the arbitrary oriented axis is mathematically represented by the following sequence of operations

$$\psi(\mathbf{r},t_{i+1})=D^{\dagger}(\beta)\cdot U_I(\mathbf{r},t_i)\cdot D(\beta)\cdot\psi(\mathbf{r},t_i), \tag{20}$$

where $U_I(\mathbf{r},t_i)$ denotes the propagation of the wave function in the parallel orientation due to the field alone. The above propagation scheme for arbitrary orientation of the polarization axis, exhibits the strength of the present approach since it allows us to perform the calculations very efficiently. In a parallel orientation, the system is cylindrically symmetric, and hence, the azimuthal quantum number is preserved, $\Delta m=0$. This selection rule allows the matrix representation of the EM field operator [Eq. (A7)] to take a block diagonal form by m. This is no longer true for arbitrary oriented configurations of the field polarization and the molecular axis. First order transitions change the azimuthal quantum number by one due to field components perpendicular to the z axis. It is therefore impossible to obtain a block diagonal form of the EM field matrix in the molecular frame. However, by rotating the system by the Euler rotation angle β into the laboratory frame, we guarantee that the azimuthal component of the transformed wave function preserves its value for transitions due to the EM field operator. Then, in this laboratory frame the matrix again can obtain a block-diagonal form in terms of the azimuthal quantum number and the calculation proceeds as in the parallel case. All the advantages of the block-diagonal structure are exploited for a highly effective propagation scheme [31].

IV. CALCULATION OF OBSERVABLES

The radial probability current of the time-dependent wave function $(j_r(\mathbf{r},t)=\hat{\mathbf{r}}\cdot\mathbf{j}(\mathbf{r},t)=\hat{\mathbf{r}}\cdot\mathrm{Im}[\psi^{\star}(\mathbf{r},t)\nabla\psi(\mathbf{r},t)])$ in terms of our spherical basis expansion is given by

$$j_r(\mathbf{r},t)=\frac{1}{r^2}\,\mathrm{Im}\sum_{lm,l'm'}f^{\star}_{lm}(r,t)\left.\frac{\partial f_{l'm'}}{\partial r}\right|_{(r,t)}Y^{\star}_{lm}(\Omega)Y_{l'm'}(\Omega). \tag{21}$$

By use of the continuinity equation $[\nabla\cdot\mathbf{j}(\mathbf{r},t)+\partial\rho(\mathbf{r},t)/\partial t=0]$, it follows that $j_r(r_0,\Omega,t)r_0^2d\Omega$ provides the number of electrons moving outwards, per unit time, within a solid angle $d\Omega=\sin\theta d\theta\, d\phi$ through a spherical surface placed at some distance r_0.

A. Angular distribution

By evaluating the probability current at the distance r_0, and integrating over time up to time t, we obtain the angular distribution from the formula

$$\frac{dP}{d\Omega}(\mathbf{r},t)=\mathrm{Im}\int_{t_0}^{t}dt'\,r_0^2 j_r(r_0,\Omega,t'). \tag{22}$$

The time t is chosen large enough that all radial outgoing flux has passed the point of observation. The distance r_0 is chosen neither close to the central region nor to the box boundaries.

B. Ionization yield

The total ionization yield can be obtained by either of the following methods.

1. Use of the probability current

By integration of Eq. (22) over the angular variables we obtain the ionization yield at time t as

$$P(t)=\int_{t_0}^{t}dt'\,\mathrm{Im}\left[\sum_{lm}f_{lm}(r_0,t')\left.\frac{\partial f_{lm}}{\partial r}\right|_{r_0,t'}\right]. \tag{23}$$

2. Use of absorbing potential

In the present approach the molecule is artificially placed inside a sphere of radius r_b, by forcing the wave function to be zero at this boundary. Physically this corresponds to the case of an infinite high potential at the box boundary. The placement of the system in a box, might be a source of artificial complications with the most prominent the unphysical reflection of the time-dependent wave function at the boundaries. To overcome this problem one solution is the implementation of an absorbing boundary throughout the inner region of the box, which mathematically is achieved through the addition of an imaginary potential into the Hamiltonian by the substitution $V(\mathbf{r},t)\rightarrow V(\mathbf{r},t)-iW(r)$. In this work we use

$$W(r)=-\frac{1}{\tau}\ln\left\{1-\cos^{p}\left[\frac{\pi}{2}\left(1-\frac{r}{r_b}\right)\right]\right\}, \tag{24}$$

where p is a parameter that affects the "smoothness" of the imaginary potential. In the present case we have chosen $p=50$. It is obvious from the chosen form of the absorbing potential that absorption is practically absent at the central

region of the system $[W(r)\to 0$ for $r\to 0]$, as it should be, while it is complete when the particle approaches the box boundaries $[W(r)\to\infty$ for $r\to r_b]$. The role of imaginary potential is twofold here. It not only solves the technical problem of the artificial scattering but also it can be used as a method to describe the ionization process. This imaginary potential removes smoothly the flux which approaches the boundaries, affecting only the continuum part of the wave function. Therefore, the loss of norm of the wave function is interpreted as ionization of the system.

In the present split-operator formulation the introduction of the absorbing potential acts as a mask function that damps the wave function at large distances, $\sim\exp(-W(r)\tau)\psi(\mathbf{r},t)$. We note in passing that whenever we calculate angular distributions in presence of the absorbing potential we choose as r_0 a radial distance where absorption is negligible. We make this choice of r_0 in order to avoid the complications introduced by the continuity equation $\nabla\cdot j(\mathbf{r},t)+\partial\rho(\mathbf{r},t)/\partial t=2W(\mathbf{r})\rho(\mathbf{r},t)$ in the presence of an absorbing potential.

C. Photoelectron energy spectrum

We calculate the photoelectron energy spectrum (PES) by taking the Fourier transform (FT) of the autocorrelation (AC) function of the time-dependent wave function $\psi(t)$. The AC function after the end of the pulse is given by

$$C(t)=\langle\psi(\mathbf{r},T)|\psi(\mathbf{r},T+t)\rangle, \tag{25}$$

where the brackets denote integration ovel all the spatial variables. The FT of the AC function, as a method for the determination of the position of the bound eigenenergies and eigenstates of a time-dependent Hamiltonian was used [57,58] in studying the hydrogen atom placed in a static electric and magnetic field [57,58], and for the determination of the population remained in the bound states after irradiation of H_2^+ with a laser pulse [20,25]. In the present case we have extended the method to the determination of the population of the continuum states [52]. To this end, we exploit the fact that since the Hamiltonian is represented on a radial grid in a sphere of radius r_b, supplemented with vanishing boundary conditions $f(0,t)=f(r_b,t)=0$, the positive energy spectrum (continuous spectrum) becomes discrete. This allows us to treat the bound and the continuous spectral decomposition of the time-dependent wave function in a unified way. To see formally how the AC function is related with the energy distribution function of $\psi(\mathbf{r},t)$ we expand the latter in the eigenstate basis $\phi_E(\mathbf{r})$ as

$$\psi(\mathbf{r},t)=\sum\!\!\!\!\!\!\int dE\, b(E)\phi_E(\mathbf{r})e^{-iEt} \tag{26}$$

with $b(E)$ describing the energy distribution of $\psi(\mathbf{r},t)$ onto the eigenstates of the field-free Hamiltonian and the symbol $\sum\!\!\!\!\!\!\int$ denoting expansion over the bound and the continuous spectrum. Then by substitution of the above expansion to Eq. (25) we obtain

$$C(t)=\sum\!\!\!\!\!\!\int dE\, b(E)\langle\psi(\mathbf{r},T)|\phi_E(\mathbf{r})\rangle e^{-iEt}. \tag{27}$$

By taking the Fourier transform of the above expansion at energy $E>0$ as $S(E)=(1/2\pi)|\int dt\, C(t)\exp(iEt)|$ we end with

$$S(E)=|b(E)\langle\psi(\mathbf{r},T)|\phi_E(\mathbf{r})\rangle|=|b(E)|^2. \tag{28}$$

In the last equality we have exploited that from Eq. (26) holds $\langle\phi_E(\mathbf{r})|\psi(\mathbf{r},t)\rangle=b(E)\exp(-iEt)$.

In practice we take the following Fourier transform of the AC function,

$$S(E,\tau)=\frac{2}{\tau}\left|\int_T^{T+\tau} dt\, C(t)h(t)e^{iEt}\right|, \tag{29}$$

where T denotes the pulse length and where $h(t)=[1-\cos(2\pi(t+T)/\tau)]/2$ is a Hanning window. The above transformation results in a series of peaks with maxima very close to the discrete eigenenergies positions, depending on the time length τ. From this finite-spectral function we extract the discrete eigenenergy positions (E_n) as well as the respective weights $|b(E_n)|^2$ up to a phase factor, allowing as to calculate the photoelectron energy spectrum. Details of the present approach with applications to ionization of hydrogen and molecular hydrogen ion are presented elsewhere [52].

V. RESULTS AND DISCUSSION

The results presented here are obtained with a box radius of $r_b=120$ a.u. The number of radial grid points is $n_r=4096$ which ensures that the initial ground state orbital is satisfactorily converged as we demonstrate below. Furthermore, the results shown in the figures are converged with $l_{\max}=8$ in the sense that they remain invariant increasing $l_{\max}$ from 6 to 8. Also by inspection of the angular momentum content, we see that the population of $l=8$ is vanishing after the pulse. As we showed in Fig. 1, the electronic binding energy obtained under these potentials, is fairly accurate at the equilibrium distance. The accuracy of the calculated ground state is thus sufficient for our purposes.

After having constructed the effective Hartree-Fock potential of H_2, we proceed to the SAE approximation and examine the behavior of the active electron under the external EM field. The EM field, linearly polarized along the $\hat{\mathbf{e}}$ unit vector, is characterized by the vector potential

$$\mathbf{A}(t)=\hat{\mathbf{e}}A_0\sin^2(\pi t/T)\cos(\omega t), \tag{30}$$

where $A_0=\sqrt{I_0}/\omega^2$, I_0 is the peak intensity and ω is the frequency. The electric field is obtained as $\mathbf{E}(t)=-\partial_t\mathbf{A}(t)$. We present results for photon energies of $\omega=20$ eV ($\sim$13th harmonics of Ti:sapphire laser) and $\omega=10.85$ eV ($\sim$7th harmonic of Ti:sapphire laser). The chosen intensities are rather modest $(I_0=10^{13}$ W/cm$^2)$ in order to ensure that nonperturbative effects do not play any role as well as due to the availability of such sources nowadays [59–61]. The choice of UV photons and fairly low intensities means that the quiver motion of the continuum electron, due to the ponderomotive potential field, is kept low. This allows us to use manageable boxes for the present calculations.

A. Alignment dependent one- and two-photon ionization yields

In Fig. 2, we present ionization yields for two different photon energies at the peak intensity $I_0=10^{13}$ W/cm^2 as a

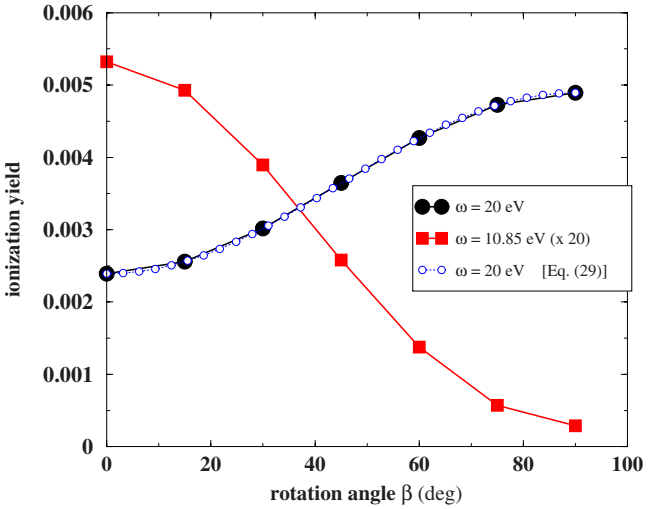

FIG. 2. (Color online) Ionization yields as a function of the orientation angle of field polarization vector with the molecular axis. Data are shown for two photon energies. The data for the $\omega=10.85$ eV case are multiplied by a factor of 20 for visualization reasons.

function of the rotation angle β. The intensity is weak enough to ensure that in the case of the 20 eV photon the ionization yield is dominated by single-photon absorption while in the case of ionization by 10.85 eV photons is dominated by two-photon processes. In both cases the final continuum states that can be reached do not include any autoionizing states of H_2. The behavior of these two cases is different. In the single-photon case, the perpendicular ionization yield is larger than the parallel yield by a factor of ~ 2. The opposite behavior is observed in the case of two-photon absorption.

Let us now give an explanation of the behavior for the single-photon absorption. Since the ground state orbital of the molecular hydrogen is of $1\sigma_g$ type and the field is linearly polarized we can have transitions into continuum states where the azimuthal quantum number changes as $\Delta m=0, \pm 1$. In the parallel orientation we can only have $\Delta m=0$ thus allowing only σ transitions to occur as $\sigma_g \rightarrow \sigma_u$. In the perpendicular orientation only $\Delta m=\pm 1$ (π transitions) transitions are allowed, $\sigma_g \rightarrow \pi_u$. Both types of transitions may occur for orientation angles between 0° and 90°. As we show in Appendix C, we can predict the alignment dependence of the yield simply by knowing the value of the π and σ transition dipole moments, or equivalently, the ionization yield for perpendicular $Y_\perp$ and parallel $Y_\parallel$ orientation as

$$Y(\beta) = Y_\parallel \cos^2 \beta + Y_\perp \sin^2 \beta. \tag{31}$$

In Fig. 2 we also show the result of the above expression (opaque circles) and find excellent agreement with the data calculated from the full time-dependent calculation. In Ref. [17] Semenov and Cherepkov give a value of the cross section for the σ transitions ($\beta=0°$) of about 1.977 Mb and for the π transitions ($\beta=90°$) 4.904 Mb. Thus our ratio of perpendicular to parallel orientation yield $Y(\beta=90°)/Y(\beta=0°) \sim 4.9\times 10^{-3}/(2.4\times 10^{-3})=2.04$ is in quite good agreement with the ratio of the π to σ single-photon cross section at $\omega=20$ eV, $\sigma_1(\pi)/\sigma_1(\sigma) \sim 2.48$.

Now we turn to the results for the ionization yield by photons of energy $\omega=10.85$ eV corresponding to nonresonant two-photon transition (filled squares). Though, one can think along the lines of the analysis presented for the single-photon ionization, the situation in the two-photon case is already much more complicated. Two-photon transitions now have a larger number of paths to reach the final state, and thus interference effects may play a role. For parallel orientation, we have $\Delta m=0$ and the path, starting from the ground state is, $\sigma_g \rightarrow \sigma_u \rightarrow \sigma_g$. In a perpendicular orientation scheme, we have $\Delta m=\pm 1$, thus allowing paths as $\sigma_g \rightarrow \pi_u \rightarrow \sigma_g$ and $\sigma_g \rightarrow \pi_u \rightarrow \delta_g$. For arbitrary orientations we have additional paths due to combination of σ and π transitions that may lead to final states having π_g symmetry in addition to σ_g and δ_g. For instance, two-photon transitions to π_g final states can occur as $\sigma_g \rightarrow \sigma_u \rightarrow \pi_g$ or $\sigma_g \rightarrow \pi_u \rightarrow \pi_g$. The fact that in the perpendicular and the parallel orientation do not exist final states as π_g do not allow to us to derive a similar formula for the two-photon ionization yield as a function of the orientation angle as the one obtained for the single-photon case [Eq. (31)]. In Ref. [62] Apalategui and Saenz calculated the two-photon generalized cross section by lowest-order perturbation theory (LOPT) for parallel and perpendicular orientation: $\sigma_2^\parallel=8\times 10^{-51}$ W/cm^2 and $\sigma_2^\perp=4.5\times 10^{-51}$ W/cm^2, respectively. Thus the decrease in ionization yield from parallel to perpendicular orientation is in agreement with our time-dependent results, though the ratio in the case of LOPT calculations ($\sigma_\parallel/\sigma_\perp \sim 1.8$) is much lower than our results $Y_\parallel/Y_\perp \sim 20$. Though we are not able to conclude about this discrepancy, we mention that the value of this ratio was changed depending on the number of partial waves retained in the calculation of the initial state. This, possibly, suggests that a convergent calculation of the effective term in the Hamiltonian (the electron-electron Coulombic interaction) should be considered not only in terms of the ground state energy obtained, but also in terms of the quality of the wave function. The latter, for instance, in the presence of an external field can affect the results through the dipole transition operator that enters into the calculations.

B. Photoelectron energy spectra

In Fig. 3 we present for parallel orientation ($\beta=0°$) the photoelectron energy spectrum for the ionization of H_2 by an external field given by Eq. (30) with photon energy $\omega=20.15$ eV, peak intensity $I_0=10^{13}$ W/cm^2, 36 field cycles, and the polarization axis along the molecular axis. We have chosen three different boxes to produce the PES, $r_b=60$, 62.5, and 65 a.u. with no absorbing potential present. After the end of the pulse, the wave function was propagated for 250 field cycles with a time step of 0.02 a.u. We calculate a partial-wave decomposed PES following a procedure described in detail in [52]. Briefly, we exploit the orthogonalization properties of the spherical harmonics, $\langle Y_{lm}|Y_{l'm'}\rangle = \delta_{ll'}\delta_{mm'}$, and write the AC function as $C(t)=\Sigma_{lm}C_{lm}(t)$ with

$$C_{lm}(t) = \langle f_{lm}(T)|f_{lm}(T+t)\rangle,$$

with $\langle\cdot|\cdot\rangle$ denoting integration only over the radial variable. The above decomposition allows us to investigate separately

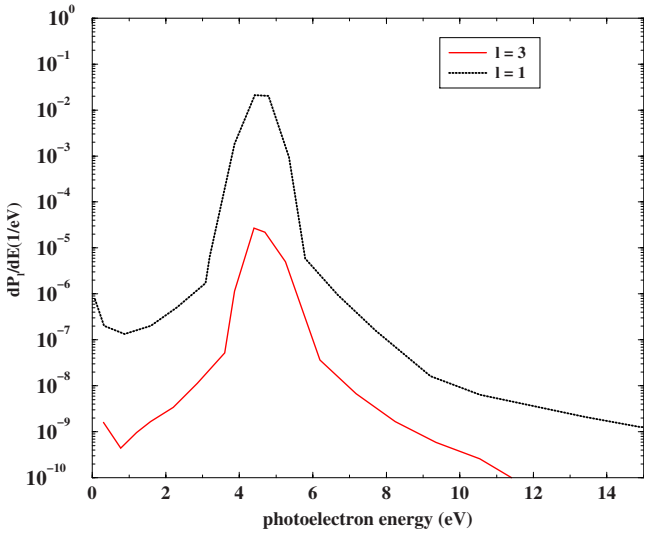

FIG. 3. (Color online) Partial photoelectron energy spectra for ionization of H_2 with photon energy $\omega=20.15$ eV and parallel orientation, $\beta=0°$.

the contribution of each $C_{lm}(t)$ to the total AC function $C(t)$ and eventually the contribution of each partial PES dP_{lm}/dE to the total PES. Therefore we obtain the PES by performing the FT to the partial AC function $C_{lm}(t)$ to obtain $S_{lm}(E,\tau)$, given as

$$S_{lm}(E,\tau)=\frac{2}{\tau}\left|\int_{T}^{T+\tau}dtC_{lm}(t)h(t)e^{iEt}\right|. \tag{32}$$

From the function $S_{lm}(E,\tau)$ we determine the discrete eigenenergies E_{nl} [and therefore the density of states by approximating it as $\rho(E_{nl})=2/|E_{n+1,l}-E_{n-1,l}|$]. The total spectrum can be obtained if we sum over the various partial PES shown in Fig. 3. In this figure we present only the dominant ionization channels p and f. In a parallel orientation only σ transitions can occur; thus $m=0$. The dominant channel of the first above-threshold ionization (ATI) peak appears to be the $p(l=1)$ channel and then the $f(l=3)$ channel. At the highest position of the ATI peak (photoelectron energy of about $\sim$5 eV) the ratio of the p channel with the f channel is about 1000 in agreement with the results by Semenov and Cherepkov [17] for the same photon energy. Interestingly enough this behavior of the p and f ionization channel is the opposite to our findings for the partial PES in the case of the single-photon ionization of the molecular hydrogen ion [52].

C. Alignment dependent angular differential ionization probabilities

The differential cross section is the most complete information that can be extracted about the molecular structure since it contains contributions from the various partial waves. From Eq. (22) with $r_0=60$ a.u., we determine the angular distribution for single-photon ($\omega=20$ eV) absorption. In Fig. 4, we show the results for three different geometries $\beta=0°$ (parallel orientation) $\beta=45°$ and for $\beta=90°$ (perpendicular orientation). The vertical dashed curve denotes the molecular axis. The corresponding ionization yields are $2.5\times10^{-3}(\beta=0°)$, $3.5\times10^{-3}(\beta=45°)$, and $4.9\times10^{-3}(\beta=90°)$. The shape in parallel orientation is a sym-

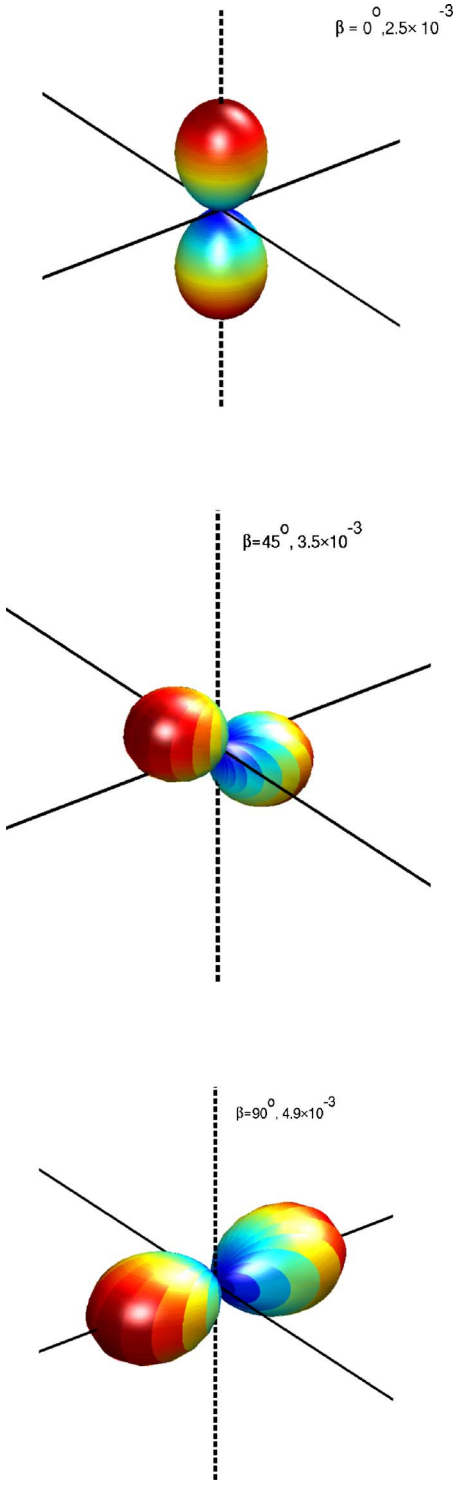

FIG. 4. (Color online) Angular distributions of the ejected electron for three different orientations of the polarization axis of the field ($\beta=0°,45°,90°$ and $\alpha=\gamma=0°$) with respect to the molecular axis and at a photon energy $\omega=20$ eV. For each orientation we also show the corresponding ionization yield. The dotted line is along the molecular axis.

metric p shape with the two lobes directed along the polarization axis. This reflects the fact that σ transitions to $l=3$ (f-waves) (or higher) partial waves are negligible compared with σ transitions to $l=1$ (p-waves), consistent with the partial PES shown in Fig. 3. In the perpendicular geometry only the π transitions contribute and again the shape is like a p partial wave. As in the parallel geometry, the reason is that π transitions to higher partial waves are much smaller in magnitude. Any deviation from this p-like shape would be the sign of population of higher partial waves [17]. In the case of $\beta=45°$, we also see a p-shape directed along the polarization axis, since both σ and π transitions contribute mainly to the $l=1$ partial wave.

In Fig. 5 we show the photoelectron angular distribution in the case of photon energy $\omega=10.85$ eV, corresponding to two-photon absorption. The corresponding ionization yields in the three geometries are $5.4\times10^{-3}(\beta=0°)$, $2.5\times10^{-3}(\beta=45°)$, and $2.5\times10^{-4}(\beta=90°)$. Let us first analyze the situation in the parallel orientation. The transitions are then only of σ type and the ionization path in terms of the symmetry of the final state is $\sigma_g\rightarrow\sigma_u\rightarrow\sigma_g$. In contrast to the single-photon case, there is an appreciable probability for ejection along the direction perpendicular to the polarization axis. The shape of the angular distribution is largely independent of the alignment angle.

VI. CONCLUSIONS

We have presented a time-dependent *ab initio* approach for the strong-field ionization of H_2 oriented at an arbitrary angle with respect to the external field in terms of the TDHF approach and the single-active electron approximation. In the future this approach suggest a systematic way of studying more complex diatomic molecular systems such as N_2 and O_2. Explicitly, what we have in mind is to perform a Hartree-Fock calculation of the doubly charged molecular ion. This will produce an effective potential replacing $Z_A/r_{iA}+Z_B/r_{iB}$ in Eq. (1). With this new effective potential, we may take over the formulation of Sec. II and establish a consistent single-electron model. How well such a procedure works for the molecular case remains to be seen but the results obtained by such a method in the atomic case are very encouraging [63]. We have made an effort to ascertain the reliability of our technique through comparison with other available theoretical results. Our chief objective in this paper was the single- and two-photon ionization from the ground state of the molecular hydrogen. We have chosen this objective for three reasons: (a) For testing our approach since interpretation of the results is easiest in low-order ionization processes, (b) due to availability of theoretical results for comparison, and (c) due to increasing interest in studies of interactions between atomic and molecular systems and strong radiation in the UV region given the emergence of new high-order harmonics and free electron laser sources.

In the implementation of our technique, it is well defined how the initial state and the propagated wave function are obtained. It is also clear how we are able to obtain results for arbitrary orientation of the EM field polarization vector and the molecular axis. A number of points have discussed such

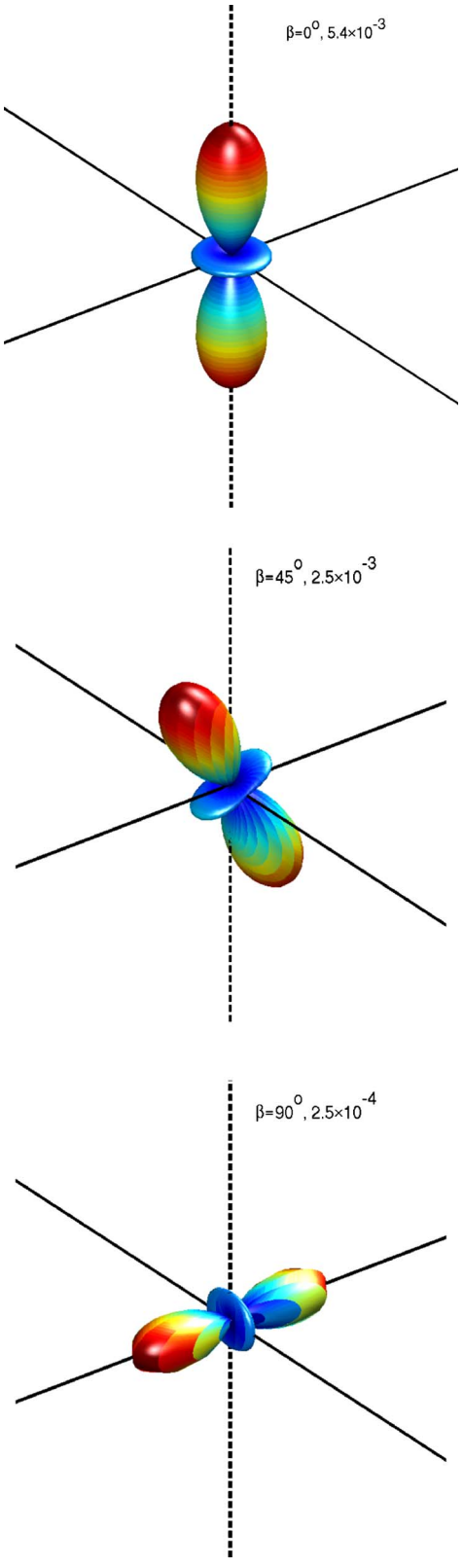

FIG. 5. (Color online) Angular distributions of the ejected electron for three different orientations of the polarization axis of the field ($\beta=0°,45°,90°$ and $\alpha=\gamma=0°$) with respect to the molecular axis and for a photon energy $\omega=10.85$ eV. For each orientation we also show the corresponding ionization yield. The dotted line is along the molecular axis.

as (i) extraction of the ionization yield, (ii) photoelectron energy spectra, and (iii) photoelectron angular distribution from the time dependent wave function after the end of the pulse.

In our opinion, all the above are well justified within the limits the HF approximation for the ground state and the single-active-electron approximation. Equally important, we believe that the present approach is sufficiently general to be applied to other "two-electron" diatomic systems with more complex cores. In such systems the HF and SAE approximations appear to be, probably, the most reliable and simultaneously cost effective way of studying their behavior under strong EM fields.

APPENDIX A: EXPANSION OF THE POTENTIALS AND PROPAGATION IN THE SPHERICAL HARMONIC BASIS

In this appendix we give the details of the time propagation induced by the various operators that we have splitted the total Hamiltonian into. According to Eqs. (14)–(17) the subpropagators correspond to the radial kinetic operator, the centrifugal operator as well as the molecular, direct and the external EM field operator. The propagation methods used for the radial kinetic and centrifugal operators (Secs. A 1 and A 2) are identical to the methods outlined in Ref. [58] and are included here for completeness.

1. Radial kinetic operator

The radial kinetic operator is independent of angular variables and acts on the radial wave functions $f_{lm}(r,t)$ individually. The radial functions are written as a vector $\mathbf{f}_{lm}(t) = \{f_{lm}(r_1,t), f_{lm}(r_2,t), \cdots f_{lm}(r_{n_r},t)\}^T$, where we assume that we know the function on n_r equidistant grid points extending to the radius r_b. If we write U_r as a matrix representation and let F be a unitary transformation that diagonalizes U_r, we find the action of the radial kinetic operator

$$\mathbf{U}_r \cdot \mathbf{f}_{lm}(t) = \mathbf{F}^\dagger \cdot \mathbf{F} \cdot \mathbf{U}_r \cdot \mathbf{F}^\dagger \cdot \mathbf{F} \cdot \mathbf{f}_{lm}(t). \tag{A1}$$

We recognize F as being the discrete Fourier transform with matrix representation $[\mathbf{F}]_{ji} = \exp(-ik_j r_i)/\sqrt{n_r}$, where the discrete momenta are $\{k_j = 2\pi(j-1)/r_b | j = 1, \cdots, n_r\}$. The diagonal form of U_r is then $[\mathbf{F} \cdot \mathbf{U}_r \cdot \mathbf{F}^\dagger]_{jj} = e^{-i(k_j^2/2)(\pi/2)}$. Since the wave function must be finite at the origin, we see from Eq. (13) that the radial functions must vanish when $r=0$. We can fulfill this boundary condition by replacing the Fourier transformations by sine transformations which also diagonalize the radial kinetic operator.

2. Centrifugal operator

Propagation of the wave function by the U_l operator is trivial since it is diagonal in a spherical basis. In each time step the radial function $f_{lm}(r,t)$ simply acquires a phase

$$U_l f_{lm}(r,t) = e^{-i[l(l+1)/2r^2](\pi/2)} f_{lm}(r,t). \tag{A2}$$

3. Potential operators

Since we work in spherical harmonics representation it is convenient to express all potentials in terms of multipoles

$$V^{(i)}(\mathbf{r},t) = \sum_{LM_L} u^{(i)}_{LM_L}(r,t) Y_{LM_L}(\theta,\phi), \tag{A3}$$

where the superscript i may stand for either M for static potential of the nuclei, D for the direct interelectronic potential, or I for the field interaction.

The potentials are written as matrix representations in the spherical harmonics basis with the elements

$$V^{(i)}_{lm,l'm'}(r,t) = \sum_{LM_L} C_{LM_L}(lm,l'm') u^{(i)}_{LM_L}(r,t), \tag{A4}$$

with $C_{LM_L}(lm,l'm') = \langle lm | Y_{LM_L} | l'm' \rangle$ being the angular factor that mixes different spherical harmonics components through the multipole potentials. The spatial and parity symmetry properties of the potentials determine the nonvanishing matrix elements of the angular factor, allowing us to derive the radial multipole potential for each specific case.

a. Nuclear potentials

Let us now derive the expressions for $u^{(M)}_{LM_L}(r)$ for the case of molecular hydrogen, where the two protons are located on the z-axis at $\pm R/2$. The charge distribution, and hence the electrostatic potential, is then azimuthally symmetric, namely $V(r,\theta,\phi) = V(r,\theta,\phi=0)$ and inversion symmetric $V(\mathbf{r}) = V(-\mathbf{r})$. The symmetries imply that only multipoles with $M_L = 0$ and $L = 0, 2, ..$ can be nonzero. The nonzero multipoles are easily evaluated as

$$u^{(M)}_{L0}(r,t) = -2\sqrt{\frac{4\pi}{2L+1}} \frac{r_<^L}{r_>^{L+1}}, \quad L \text{ even}, \tag{A5}$$

where $r_> = \max(r, R/2)$, $r_< = \min(r, R/2)$.

b. Direct interelectronic potential

By expanding the density of the inactive electron in partial waves [Eq. (13)] and substitute in Eq. (6), we derive the multipole radial potentials of the direct potential $V^{(D)}(\mathbf{r},t)$

$$u^{(D)}_{LM_L}(r,t) = \frac{4\pi}{2L+1} \int dr' \frac{r_<^L}{r_>^{L+1}} \Phi_{LM_L}(r',t),$$

$$\Phi_{LM_L}(r,t) = \sum_{ll'm} C_{LM_L}(lm,l'm) f^*_{lm}(r,t) f_{l'm}(r,t), \tag{A6}$$

with $r_> = \max(r,r')$, $r_< = \min(r,r')$. In the special case when the inactive electron occupies an orbital with azimuthal quantum number m and definite parity, the charge density $|\psi(\mathbf{r},t)|^2$ is azimuthal and inversion symmetric. Correspondingly, the direct potential only generates multipoles with $M_L = 0$ and L even as in the case for the nuclear potential. (See Fig. 6.)

Let us now to estimate the computational cost for the direct potential. Assume that the grid is divided to n_r points. At each time step, a demand of n_r integrals, each of them consisting from an $l \times l' \times m \times n_r$ evaluations of the radial orbitals $f_{lm}(r,t)$ and $f_{l'm}(r,t)$, makes the computational scaling to be of the order of $\sim n_r^2$. However, in Appendix B we show how we can reduce the scaling to a linear dependence

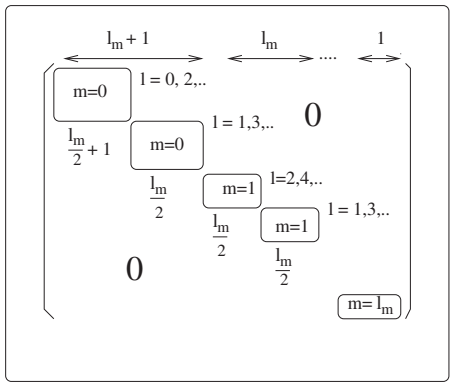

FIG. 6. Matrix representation of the nuclear and direct interelectronic potential for a homonuclear diatomic molecule. The maximum angular momentum l_m is assumed to be even. For better visualization we have omitted the blocks corresponding the negative magnetic quantum numbers.

of n_r through a recursive scheme. This consists a major gain which we wish to exploit in subsequent works beyond the present SAE approximation.

c. Electromagnetic interaction potential

The interaction operator with the EM field in the spherical basis, and in the dipole approximation for light of arbitrary polarization ($\hat{\mathbf{e}}$) is expressed (in the length gauge) as

$$V_I(\mathbf{r},t) = E(t)\hat{\mathbf{e}}\cdot\mathbf{r} = E(t)\sqrt{\frac{4\pi}{3}}\sum_{q=-1}^{1} re_q^{\star}Y_{1q}(\theta,\phi), \quad \text{(A7)}$$

where e_q are the spherical components of the polarization vector in a Cartesian coordinate system. Thus by consideration of the multipole expansion of the potentials Eq. (A4) we see that the radial part of the EM field potential is given by

$$u_{1q}^{(I)}(r,t) = e_q^{\star}\sqrt{\frac{4\pi}{3}}E(t)r, \quad \text{(A8)}$$

while the mixing angular factor is $C_{1q}(lm;l'm') = \langle lm|Y_{1q}|l'm'\rangle$. In the present case we use linearly polarized light, thus $q=0$ [52].

The EM interaction potential of a molecule in a linearly polarized light along the molecular axis couples only states with equal magnetic quantum number. The general scheme of performing the propagation of the radial wave functions f_{lm} subject to the potential $V_I(\mathbf{r},t)$ is as follows. The matrix representation of $V_I(\mathbf{r},t)$ is nondiagonal in the spherical basis $\langle lm|V_I(r,t)|l'm'\rangle = (4\pi/3)^{1/2}E(t)r\delta_{mm'}\langle lm|Y_{10}|l'm\rangle$. In order to take its evolution action $[\exp(-iV_I(\mathbf{r},t)\tau)]$, we diagonalize the angular matrix defined by the elements $[\mathbf{C}_{10}]_{lm,l'm} = \langle lm|Y_{10}|l'm\rangle$ by the orthogonal transformation $\mathbf{C}_{10} = \mathbf{C}_I\cdot\mathbf{C}_d\cdot\mathbf{C}_I^{\dagger}$. We arrange the f_{lm} wave functions by the vector $\mathbf{f}$ for each fixed value of r such that the matrix representation of V_I is block diagonal in terms of the azimuthal quantum number m. Then we propagate the wave function as

$$\mathbf{U}(t,\tau)\cdot\mathbf{f}(r,t) = \mathbf{C}_I\cdot e^{-i\mathbf{V}_d(r,t)\tau}\cdot\mathbf{C}_I^{\dagger}\cdot\mathbf{f}(r,t). \quad \text{(A9)}$$

In the above expression $\mathbf{V}_d(r,t) = (4\pi/3)^{1/2}E(t)r\mathbf{C}_d$ is diagonal and exponentiation is performed with no cost by simply taking the exponents of the diagonal elements. The key point here is that though the interaction potential is time dependent the diagonalization and the calculation of the matrices $\mathbf{C}_I$ and $\mathbf{C}_d$ is performed only once. At each time step a block diagonal multiplication of maximum dimension $(l_{\max}+1)$ is performed in order to obtain the propagated wave function.

d. Computational considerations

In the factorization scheme [Eq. (14)], both the radial kinetic and centrifugal operators act independently on each of the partial waves, represented by the radial functions $f_{lm}(r,t)$. In other words, the evolution of each $f_{lm}(r,t)$ is completely independent of the evolutions all others radial functions. This allows for a very efficient propagation of the wave function. This is no longer true when we have to propagate the wave function by the potential $V(\mathbf{r},t)$. The time evolution of the $f_{lm}(r,t)$ is now coupled with the time evolution of the other partial waves $f_{l'm'}(r,t)$ since generally $V(\mathbf{r},t)$ has a nondiagonal representation on the spherical harmonic basis. The general scheme of performing the propagation of the radial wave functions f_{lm} subject to the potential $V(\mathbf{r},t)$ is presented in detail in Ref. [31].

APPENDIX B: CALCULATION OF THE RADIAL SLATER INTEGRAL

Our intention is to calculate the radial multipole potential as it given in Eq. (A6). These types of integrals are known as Slater integrals and occur very often in atomic and molecular structure calculations. If we define, $p^{(k)}(r) = r^2r^k\Phi_k(r,t)$ and $q^{(k)}(r) = r^2\Phi_k(r,t)/r^{k+1}$ the Slater expression for the direct potential is written as

$$Y^{(k)}(r) = \frac{1}{r^{k+1}}P^{(k)}(r) + r^kQ^{(k)}(r), \quad Y^k(0) = 0. \quad \text{(B1)}$$

where we have defined $P^{(k)}(r) = \int_0^r dr' p^{(k)}(r')$ and $Q^{(k)}(r) = \int_r^{\infty} dr' q^{(k)}(r')$. Each of the previous integrals in a numerical integration scheme is approximated as $P_i^{(k)} = \Sigma_{j=1} w_j p_j^{(k)}$ and $Q_i^{(k)} = \Sigma_{j=1} w_j q_j^{(k)}$. The index $'i'$ stands for the boundary point $r_i = r$ in the integrals $P^{(k)}(r)$, $Q^{(k)}(r)$. Furthermore, we have suppressed the time dependence since the present procedure is assumed to repeated at each time step. Thus time is constant during the evaluation of the Slater integrals $Y^{(k)}(r)$. The recursive scheme is based on the fact that the value of the two integrals $P_i^{(k)}$ and $Q_i^{(k)}$ are not independent each other, but related through the boundary point r. Given that for each numerical quadrature we may write

$$P_{i+1}^{(k)} = P_i^{(k)} + w_{i+1}p_{i+1}^{(k)}, \quad \text{(B2)}$$

$$Q_{i+1}^{(k)} = Q_i^{(k)} - w_i q_i^{(k)}. \quad \text{(B3)}$$

From the above equations it is evident that we can calculate the Slater integral at position r_{i+1} as

$$Y_{i+1}^{(k)} = \frac{1}{r_{i+1}^{k+1}}[P_i^{(k)} + w_{i+1}p_{i+1}^{(k)}] + r_{i+1}^{k}[Q_i^{(k)} - w_i q_i^{(k)}], \quad \text{(B4)}$$

if we know the integrals $P_i^{(k)}$, $Q_i^{(k)}$ at the position r_i. Therefore, by starting from $i=1$, where $r_1=0$ we can recursively calculate the n_r integrals by only evaluating the integral for $Q_1^{(k)}=Q^{(k)}(0)=\int_0^\infty dr' q^{(k)}(r')$ and $P_1^{(k)}=P^{(k)}(0)=0$. The next value for $i=2$ is calculated from the recursive relation Eq. (B4) by using the values of the integrals $P_1^{(k)}$, $Q_1^{(k)}$ and $p_2^{(k)}$ and $q_1^{(k)}$. This way we evaluate the next n_q-2 integrals by having, in practice, evaluated only one integral, namely the $Q_1^{(k)}$ integral.

APPENDIX C: ALIGNMENT DEPENDENT SINGLE-PHOTON IONIZATION

In this appendix we calculate the alignment dependent ionization yield for a single-photon transition from an initial σ_g state. By assuming that the ionization yield, for a fixed orientation scheme at angle β, is proportional to the differential cross section we next consider the single photon differential cross section which in the length gauge is written as

$$\frac{d\sigma}{d\Omega_{\mathbf{k}}} = 4\pi^2\alpha\omega|D(\mathbf{k})|^2, \quad \text{(C1)}$$

where $D(\mathbf{k})=\langle\psi_{\mathbf{k}}^{(-)}(\mathbf{r})|\hat{\mathbf{e}}\cdot\mathbf{r}|\psi_0(\mathbf{r})\rangle$ is the matrix element between the initial ψ_0 and the final state $\psi_{\mathbf{k}}^{(-)}$ and α is the fine structure constant. The final state $\psi_{\mathbf{k}}^{(-)}$ is an ingoing-wave, energy normalized, continuum state of asymptotic momentum $\mathbf{k}$, which in a partial wave expansion reads

$$\psi_{\mathbf{k}}^{(-)}(\mathbf{r}) = \sum_{lm} \phi_{k,lm}(\mathbf{r})Y_{lm}^{\star}(\hat{\mathbf{k}}), \quad \text{(C2)}$$

where $\phi_{k,lm}$ are continuum channel wave functions.

It is convenient to evaluate the matrix element in the molecular frame. For an alignment angle β between the polarization axis and the molecular axis, the polarization vector is given in the molecular frame as $\hat{\mathbf{e}}=\sin\beta\hat{\mathbf{x}}+\cos\beta\hat{\mathbf{z}}$. By standard translation between Cartesian and spherical components, we obtain

$$\hat{\mathbf{e}}\cdot\mathbf{r} = r\sqrt{\frac{4\pi}{3}}\left(\cos\beta Y_{10}(\hat{\mathbf{r}}) + \frac{\sin\beta}{\sqrt{2}}[-Y_{11}(\hat{\mathbf{r}}) + Y_{1-1}(\hat{\mathbf{r}})]\right).$$

If we assume that the initial state is a σ_g state with angular momentum projection $m_0=0$, we see from the above expansion that only $m=0,\pm1$ components of the partial wave expansion (C2) can contribute to the matrix element. The matrix element in Eq. (C1) can therefore be written as a sum of three terms

$$D(\mathbf{k}) = \cos\beta d_\sigma(\mathbf{k}) + \frac{\sin\beta}{\sqrt{2}}[-d_{\pi^+}(\mathbf{k}) + d_{\pi^-}(\mathbf{k})],$$

where

$$d_\sigma(\mathbf{k}) = \sqrt{\frac{4\pi}{3}}\sum_l \langle\phi_{k,l0}(\mathbf{r})|rY_{10}(\hat{\mathbf{r}})|\psi_0(\mathbf{r})\rangle Y_{l0}(\hat{\mathbf{k}}),$$

$$d_{\pi^\pm}(\mathbf{k}) = \sqrt{\frac{4\pi}{3}}\sum_l \langle\phi_{k,l,\pm1}(\mathbf{r})|rY_{1,\pm1}(\hat{\mathbf{r}})|\psi_0(\mathbf{r})\rangle Y_{l,\pm1}(\hat{\mathbf{k}}).$$

The total cross section, integrated over all directions of the outgoing electron, is now obtained as a function of β

$$\sigma(\beta) = 4\pi^2\alpha\omega\left[\cos^2\beta\int d\Omega_{\mathbf{k}}|d_\sigma(\mathbf{k})|^2 + \frac{\sin^2\beta}{2}\int d\Omega_{\mathbf{k}}(|d_{\pi^+}(\mathbf{k})|^2 + |d_{\pi^-}(\mathbf{k})|^2)\right]. \quad \text{(C3)}$$

Note that cross terms of the type $d_\sigma^\star(\mathbf{k})d_\pi(\mathbf{k})$ vanish when we integrate over $\Omega_{\mathbf{k}}$ due to orthogonality of the spherical harmonics for different azimuthal numbers. For $\beta=0°$ and $\beta=90°$ we find the cross sections for the parallel and perpendicular geometries as

$$\sigma_\parallel = 4\pi^2\alpha\omega\int d\Omega_{\mathbf{k}}|d_\sigma(\mathbf{k})|^2,$$

$$\sigma_\perp = 4\pi^2\alpha\omega\frac{1}{2}\int d\Omega_{\mathbf{k}}(|d_{\pi^+}(\mathbf{k})|^2 + |d_{\pi^-}(\mathbf{k})|^2),$$

respectively. We finally insert the expressions above in Eq. (C3) and obtain

$$\sigma(\beta) = \cos^2\beta\sigma_\parallel + \sin^2\beta\sigma_\perp. \quad \text{(C4)}$$

According the LOPT the single-photon ionization rate at time t is related with the total cross section as $W(\beta,t)=\sigma(\beta)I(t)/\omega$, with $I(t)=E^2(t)$ the intensity profile of the EM field and ω the photon frequency. Thus the ionization yield is obtained by integration of $W(t)$ over the pulse duration to obtain $Y(\beta)=\cos^2\beta Y_\parallel+\sin^2\beta Y_\perp$ which is equivalent to Eq. (31). In the above $Y_\parallel=\sigma_\parallel I_0\tau_1/\omega$ and $Y_\parallel=\sigma_\perp I_0\tau_1/\omega$, with $\tau_1=\int_0^T dt f^2(t)$ being the effective interaction time and $f(t)$ the pulse envelope [Eq. (30)].

[1] J. H. Posthumus, Rep. Prog. Phys. **67**, 623 (2004).

[2] H. Wabnitz, A. R. B. deCastro, P. Gurtler, T. Laarmann, W. Laasch, J. Schulz, and T. Moller, Phys. Rev. Lett. **94**, 023001 (2005).

[3] A. A. Sorokin, S. V. Bobashev, K. Tiedtke, and M. Richter, J. Phys. B **39**, L299 (2006).

[4] D. Zeidler, A. B. Bardon, A. Staudte, D. M. Villeneuve, R. Dörner, and P. B. Corkum, J. Phys. B **39**, L159 (2006).

[5] H. Niikura, F. Légaré, R. Hasbani, A. D. Bandrauk, M. Y. Ivanov, D. M. Villeneuve, and P. B. Corkum, Nature (London) **417**, 917 (2002).

[6] H. Niikura, F. Légaré, R. Hasbani, M. Y. Ivanov, D. M. Ville-

neuve, and P. B. Corkum, Nature (London) **421**, 826 (2003).
[7] A. S. Alnaser *et al.*, Phys. Rev. Lett. **93**, 183202 (2004).
[8] J. Itatani, J. Levesque, D. Zeidler, H. Niikura, H. Pépin, J. C. Kieffer, P. B. Corkum, and D. M. Villeneuve, Nature (London) **432**, 867 (2004).
[9] A. S. Alnaser, T. Osipov, E. P. Benis, A. Wech, B. Shan, C. L. Cocke, X. M. Tong, and C. D. Lin, Phys. Rev. Lett. **91**, 163002 (2003).
[10] H. Rottke *et al.*, Phys. Rev. Lett. **89**, 013001 (2002).
[11] K. C. Kulander, Phys. Rev. A **36**, 2726 (1987).
[12] F. Martin, J. Phys. B **32**, R197 (1999).
[13] P. G. Burke, J. Colgan, D. H. Glass, and K. Higgins, J. Phys. B **33**, 143 (2000).
[14] H. Bachau, E. Cormier, P. Decleva, J. E. Hansen, and F. Martin, Rep. Prog. Phys. **64**, 1815 (2001).
[15] J. Colgan, D. H. Glass, K. Higgins, and P. G. Burke, J. Phys. B **34**, 12089 (2001).
[16] J. Colgan, M. S. Pindzola, and F. Robicheaux, J. Phys. B **37**, L377 (2004).
[17] S. K. Semenov and N. A. Cherepkov, J. Phys. B **36**, 1409 (2003).
[18] C. Siedschlag and T. Pattard, J. Phys. B **38**, 2297 (2005).
[19] W. Vanroose, D. A. Horner, F. Martin, T. N. Rescigno, and C. W. McCurdy, Phys. Rev. A **74**, 052702 (2006).
[20] D. Dundas, J. F. McCann, J. S. Parker, and K. T. Taylor, J. Phys. B **33**, 3261 (2000).
[21] S. Barmaki, S. Laulan, and M. Ghalim, J. Phys. B **36**, 817 (2003).
[22] G. Lagmago Kamta and A. D. Bandrauk, Phys. Rev. A **70**, 011404 (2004).
[23] M. Awasthi, Y. V. Vanne, and A. Saenz, J. Phys. B **38**, 3973 (2005).
[24] S. Selstø, J. F. McCann, M. Førre, J. P. Hansen, and L. B. Madsen, Phys. Rev. A **73**, 033407 (2006).
[25] D. Dundas, Phys. Rev. A **65**, 023408 (2002).
[26] L.-Y. Peng, D. Dundas, J. F. McCann, K. T. Taylor, and I. D. Williams, J. Phys. B **36**, L295 (2003).
[27] A. Palacios, S. Barmaki, H. Bachau, and F. Martin, Phys. Rev. A **71**, 063405 (2005).
[28] G. LagmagoKamta and A. D. Bandrauk, Phys. Rev. A **71**, 053407 (2005).
[29] G. L. Kamta and A. D. Bandrauk, Phys. Rev. A **74**, 033415 (2006).
[30] T. K. Kjeldsen, L. B. Madsen, and J. P. Hansen, Phys. Rev. A **74**, 035402 (2006).
[31] T. K. Kjeldsen, L. A. A. Nikolopoulos, and L. B. Madsen, Phys. Rev. A **75**, 063427 (2007).
[32] M. Awasthi and A. Saenz, J. Phys. B **39**, S389 (2006).
[33] E. Goll, G. Wunner, and A. Saenz, Phys. Rev. Lett. **97**, 103003 (2006).
[34] A. Palacios, S. Barmaki, H. Bachau, and F. Martin, Phys. Rev. Lett. **96**, 143001 (2006).
[35] J. L. Sanz-Vicario, H. Bachau, and F. Martin, Phys. Rev. A **73**, 033410 (2006).
[36] R. Velotta, N. Hay, M. B. Mason, M. Castillejo, and J. P. Marangos, Phys. Rev. Lett. **87**, 183901 (2001).
[37] I. V. Litvinyuk, K. F. Lee, P. W. Dooley, D. M. Rayner, D. M. Villeneuve, and P. B. Corkum, Phys. Rev. Lett. **90**, 233003 (2003).
[38] G. Onida, L. Reining, and A. Rubio, Rev. Mod. Phys. **74**, 601 (2002).
[39] K. C. Kulander, Phys. Rev. A **38**, 778 (1988).
[40] M. S. Pindzola, D. Griffin, and C. Bottcher, Phys. Rev. Lett. **66**, 2305 (1991).
[41] J. L. Krause, K. J. Schafer, and K. C. Kulander, Chem. Phys. Lett. **178**, 573 (1991).
[42] M. S. Pindzola, T. W. Gorczyca, and C. Bottcher, Phys. Rev. A **47**, 4982 (1993).
[43] M. S. Pindzola, P. Gavras, and T. W. Gorczyca, Phys. Rev. A **51**, 3999 (1995).
[44] H. Yu and A. D. Bandrauk, J. Chem. Phys. **102**, 1257 (1995).
[45] P. Maragakis and P. Lambropoulos, Laser Phys. **7**, 1 (1997).
[46] M. Horbatsch, H. J. Ludde, and R. M. Dreizler, J. Phys. B **25**, 3315 (1992).
[47] N. E. Dahlen and R. van Leeuwen, Phys. Rev. A **64**, 023405 (2001).
[48] N. A. Nguyen and A. D. Bandrauk, Phys. Rev. A **73**, 032708 (2006).
[49] S. X. Hu, W. X. Qu, and Z. Z. Xu, Phys. Rev. A **57**, 3770 (1998).
[50] J. Caillat, J. Zanghellini, M. Kitzler, O. Koch, W. Kreuzer, and A. Scrinzi, Phys. Rev. A **72**, 012712 (2005).
[51] G. Jordan, J. Caillat, and A. Scrinzi, J. Phys. B **39**, S341 (2006).
[52] L. A. A. Nikolopoulos, T. K. Kjeldsen, and L. B. Madsen, Phys. Rev. A **75**, 063426 (2007).
[53] A. D. Bandrauk and H. Z. Lu, Phys. Rev. A **72**, 023408 (2005).
[54] J. Parker, E. S. Smyth, and K. T. Taylor, J. Phys. B **31**, L571 (1998).
[55] J. Kobus, L. Laaksonen, and D. Sundholm, Comput. Phys. Commun. **98**, 346 (1996).
[56] A. Messiah, *Quantum Mechanics* (Dover, New York, 1999).
[57] M. D. Feit, J. J. A. Fleck, and A. Steiger, J. Comput. Phys. **47**, 412 (1982).
[58] M. R. Hermann and J. A. Fleck, Phys. Rev. A **38**, 6000 (1988).
[59] N. A. Papadogiannis, L. A. A. Nikolopoulos, D. Charalambidis, G. D. Tsakiris, P. Tzallas, and K. Witte, Phys. Rev. Lett. **90**, 133902 (2003).
[60] K. L. Ishikawa and K. Midorikawa, Phys. Rev. A **65**, 043405 (2002).
[61] Y. Nabekawa, H. Hasegawa, E. J. Takahashi, and K. Midorikawa, Phys. Rev. Lett. **94**, 043001 (2005).
[62] A. Apalategui and A. Saenz, J. Phys. B **35**, 1909 (2002).
[63] L. A. A. Nikolopoulos, Phys. Rev. A **71**, 033409 (2005).